AN INNOVATIVE LIFTING-LINE MODEL FOR PROPROTORS IN AXIAL FLIGHT

Gregorio Frassoldati
Università Degli Studi Roma Tre
Leonardo Helicopters
Rome - Cascina Costa, Italy

Giovanni Bernardini
Università Degli Studi Roma Tre
Rome, Italy

Massimo Gennaretti
Università Degli Studi Roma Tre
Rome, Italy

ABSTRACT

A time-stepping, lifting-line solution algorithm, designed to predict the unsteady aerodynamics of rotorcraft blades, is presented. This method extends recently developed lifting-line techniques —originally applied to prescribed-wake and free-wake wing problems— to the realm of rotary-wing applications. The approach leverages an intrinsic time-stepping description paired with a free wake model, making it a natural fit for generic rotary-wing configurations. A key aspect of this work is the excellent correlation achieved against a fully three-dimensional Boundary Element Method for potential flows. The work presents a comprehensive validation dataset. This dataset will span a variety of applications with unsteady harmonic motions for rotors in hovering conditions and extend to airplane mode axial flight conditions of proprotors, detailing the enhancements that have been briefly outlined here.

NOTATION

*

Symbols

b Airfoil semi-chord, m

c Airfoil chord, m

k Reduced frequency

M_z Torque, Nm

N_b Number of blades

R Rotor radius, m

T Rotor thrust, N

V Velocity, m/s

$\theta_{75\%}$ Pitch angle at 75% of blade radius

ρ Air density, kg/m^3

ω Pulsation

Ω Rotor angular velocity, rad/s

*

Acronyms

BEM Boundary Element Method

KJ Kutta-Joukowski (Theorem)

KS Küssner-Schwarz (Model)

LL Lifting Line (Model)

ULLT Unsteady Lifting Line Theory

USLL Unsteady Lifting Line (Model)

INTRODUCTION

The significant influence of interactional aerodynamics on aircraft performance underscores the necessity for efficient aerodynamic modeling. This requirement is particularly critical in rotary-wing aircraft, where the inherently unsteady nature of rotor operation demands the use of specialized modeling tools.

Rotor blades, typically characterized as slender lifting surfaces optimized for hover, are often analyzed using aerodynamic models based on two-dimensional theories. These models permit extensive exploration of the design space while substantially reducing computational costs. In particular, by integrating a spanwise distribution of sectional properties with a lifting-line approach, engineers can effectively assess various configurations without resorting to complex geometry processing or meshing.

However, the traditional lifting-line theory (Refs. 1, 2) relies on assumptions that become questionable when applied to blades experiencing highly unsteady and non-uniform flow fields. As a result, there is a compelling need to reformulate the aerodynamic models to more accurately capture the dynamic interactions inherent in such conditions.

Most foundational work in unsteady aerodynamics, such as the theories developed by Theodorsen (Ref. 3) and Wagner (Ref. 4), was originally intended for fixed wings in idealized flow conditions. While these models provide analytical predictions of lift and pitching moment in unsteady flows, their assumptions are not suitable for rotor applications.

This study presents the development and application of a time-domain Unsteady Lifting-Line Theory (ULLT) for rotor analysis. The numerical investigation evaluates the model's predictions of generalized aerodynamic forces across various axial flight regimes. These results are compared with those obtained from a validated boundary element method (BEM) for three-dimensional potential flow (Refs. 5–12). A detailed description of the BEM tool and its validation as a benchmarking reference can be found in (Ref. 13).

METHOD DESCRIPTION

The model presented here is a fully unsteady lifting-line approach that considers the dynamic evolution of a vortex-lattice wake, based on its own self-induced velocity field. Sectional aerodynamic loads are computed using Küssner-Schwarz's model, with full dynamic adaptation. To complete the lifting-line formulation, the model incorporates a fourth-order representation of the unsteady Kutta-Joukowski theorem (Ref. 14).

Küssner-Schwarz Sectional Theory

To compute the aerodynamic forces on each section of the lifting body, the only formulation valid regardless of the motion of the body and the inflow distribution of the incoming wind, is the solution derived by Küssner-Schwarz (Refs. 15, 16). Other existing models are based on specific assumptions about downwash profiles, such as constant or linear distributions (Ref. 3), or hypothesize about the gust shapes encountered by the airfoil (Refs. 17–19).

To describe the Küssner-Schwarz's model, let V denote the undisturbed flow speed, and consider a coordinate system (x,z) where the origin is at the midpoint of the airfoil, the x-axis is aligned with the unperturbed flow and the airfoil, directed from the leading to the trailing edge, whereas the z-axis is positive upwards. Additionally, let b represent the airfoil's semichord and ω the angular frequency, with the key non-dimensional parameter $k = \omega b/V$, which is the reduced frequency.

Assuming the physical downwash velocity, v, as that produced by the vertical displacement, w, of the airfoil we have

$$v = V\frac{\partial w}{\partial x} + \dot{w} \tag{1}$$

with the displacement expressed as a linear combination of M shape functions

$$w(x,t) = \sum_{m=1}^{M} \psi_m(x) q_m(t) \tag{2}$$

where q_m represents the m-th generalized Lagrangian coordinate (downwash description aimed at aeroelastic applications). Rewriting Eq. (1) in the frequency domain and combining it with Eq. (2) yields

$$\tilde{v}(\xi) = \frac{V}{b}\left[\frac{\partial \tilde{w}}{\partial \xi} + ik\tilde{w}\right] = \frac{V}{b}\sum_{m=1}^{M}\left[\frac{\partial \psi_m}{\partial \xi} + ik\psi_m\right]\tilde{q}_m \tag{3}$$

where $\xi = x/b$ is the non-dimensional chordwise coordinate, with the leading and trailing edges of the airfoil corresponding to $\xi = -1$ and $\xi = 1$, respectively.

Next, for $\theta = \arccos(\xi)$ the downwash is expressed through the following cosine-series (for $N \to \infty$)

$$\tilde{v}(\xi) = V\sum_{n=0}^{N}\tilde{P}_n \cos n\theta(\xi)$$

where

$$\tilde{P}_n = -\frac{1}{\pi b}\sum_{m=1}^{M}\left[\int_{-1}^{1}\left(\frac{\partial \psi_m}{\partial \xi} + ik\psi_m\right)\frac{\cos n\theta(\xi)}{\sqrt{1-\xi^2}}\mathrm{d}\xi\right]\tilde{q}_m \tag{4}$$

Then, it is demonstrated (Refs. 15, 16) that the corresponding pressure jump distribution along the chord is given by

$$\Delta\tilde{p}(\xi) = -2\rho V^2\left[\tilde{a}_0\frac{\sqrt{1-\xi}}{\sqrt{1+\xi}} + 2\sum_{n=1}^{N}\tilde{a}_n \sin n\theta(\xi)\right] \tag{5}$$

where ρ denotes the air density and the $\tilde{a}_n$ coefficients depend on the downwash cosine-series coefficients

$$\begin{cases}\tilde{a}_0(k) = C(k)(\tilde{P}_0 + \tilde{P}_1) - \tilde{P}_1 \\ \tilde{a}_n(k) = \tilde{P}_n + ik\left(\tilde{P}_{n-1} - \tilde{P}_{n+1}\right)/2n \quad \text{for } n \geq 1\end{cases} \tag{6}$$

The pressure jump distribution can be separated into circulatory and non-circulatory components. The non-circulatory part is

$$\begin{aligned}\Delta\tilde{p}^{nc}(\xi) = -2\rho V^2 \\ \Bigg[\left(ik\sqrt{1-\xi^2}\right)\tilde{P}_0 + \left((2+ik\xi)\sqrt{1-\xi^2} - \frac{\sqrt{1-\xi}}{\sqrt{1+\xi}}\right)\tilde{P}_1 \\ +2\sum_{n=2}^{N}S_n(\xi,k)\tilde{P}_n\Bigg]\end{aligned} \tag{7}$$

where $S_n(\xi,k)$ is given by

$$\begin{aligned}S_n(\theta(\xi),k) = -\frac{ik}{2(n-1)}\sin[(n-1)\theta] + \sin[n\theta] \\ + \frac{ik}{2(n+1)}\sin[(n+1)\theta]\end{aligned} \tag{8}$$

The circulatory part is:

$$\Delta\tilde{p}^{c}(\xi) = -2\rho V^2\sqrt{\frac{1-\xi}{1+\xi}}C(k)\tilde{Q} \tag{9}$$

where $C(k)$ is the lift deficiency function formulated by Theodorsen (Ref. 3), and $\tilde{Q}$ is defined as:

$$\tilde{Q} = \tilde{P}_0 + \tilde{P}_1 \tag{10}$$

$$= -\frac{1}{\pi b} \sum_{m=1}^{M} \left[\int_{-1}^{1} \left(\frac{\partial \psi_m}{\partial \xi} + ik\psi_m \right) \sqrt{\frac{1+\xi}{1-\xi}} \mathrm{d}\xi \right] \tilde{q}_m \tag{11}$$

For a finite-state representation of the problem (useful for stability analysis and for its time-domain description for aeroservoelastic applications) a second-order rational approximation of the lift deficiency function is provided (Ref. 20)

$$C(k) = \frac{1}{2} \frac{(ik - z_1)(ik - z_2)}{(ik - \sigma_1)(ik - \sigma_2)} \tag{12}$$

where z_1, z_2 and σ_1, σ_2 denote zeros and poles, respectively. This leads to the following description of the circulatory loads component

$$\begin{cases} \Delta\tilde{p}^c(\xi) = -2\rho V^2 \sqrt{\dfrac{1-\xi}{1+\xi}} \dfrac{1}{2} \left[-k^2 - (z_1 + z_2)ik + z_1 z_2 \right] \tilde{r} \\ \left[-k^2 - (\sigma_1 + \sigma_2)ik + \sigma_1 \sigma_2 \right] \tilde{r} = \tilde{Q} \end{cases} \tag{13}$$

where $\tilde{r}$ represents an additional aerodynamic state introduced by the poles of the rational approximation of $C(k)$.
The sectional generalized aerodynamic loads, $\tilde{f}_m$, to be considered in aeroelastic applications are then obtained by projecting the pressure jump onto the set of shape functions used to express the displacement

$$\tilde{f}_m = \tilde{f}_m^c + \tilde{f}_m^{nc} = -b \int_{-1}^{1} \left[\Delta\tilde{p}^c(\xi) + \Delta\tilde{p}^{nc}(\xi) \right] \psi_m(\xi) \mathrm{d}\xi \tag{14}$$

where $\tilde{f}_m^c$ and $\tilde{f}_m^{nc}$ denote the circulatory and non-circulatory parts of the generalized aerodynamic loads, respectively.

Combining Eqs. (14), (13), (10) and rearranging them in vector form yields the following expression for the circulatory loads

$$\begin{cases} \tilde{\mathbf{f}}^c = 2b\rho V^2 \mathbf{g} \left[-k^2 - (z_1 + z_2)ik + z_1 z_2 \right] \tilde{r} \\ \left[-k^2 - (\sigma_1 + \sigma_2)ik + \sigma_1 \sigma_2 \right] \tilde{r} = \left(\mathbf{h}^T + ik\mathbf{l}^T \right) \tilde{\mathbf{q}} \end{cases} \tag{15}$$

where $\mathbf{g}$, $\mathbf{h}$, $\mathbf{l}$ are $[M \times 1]$ vectors, whose component are expressed as

$$\begin{cases} g_m = \dfrac{1}{2} \displaystyle\int_{-1}^{1} \dfrac{\sqrt{1-\xi}}{\sqrt{1+\xi}} \psi_m \mathrm{d}\xi \\ h_m = -\dfrac{1}{\pi b} \displaystyle\int_{-1}^{1} \dfrac{\sqrt{1-\xi^2}}{1-\xi} \dfrac{\partial \psi_m}{\partial \xi} \mathrm{d}\xi \\ l_m = -\dfrac{1}{\pi b} \displaystyle\int_{-1}^{1} \dfrac{\sqrt{1-\xi^2}}{1-\xi} \psi_m \mathrm{d}\xi \end{cases} \tag{16}$$

In the same way, the non-circulatory part of the generalized aerodynamic loads is obtained by the combination of Eqs. (14), (7) and (4), that provides, after rearranging in vector form

$$\tilde{\mathbf{f}}^{nc} = 2b\rho V^2 \left[-k^2 \mathbf{CB} + ik(\mathbf{CA} + \mathbf{DB}) + \mathbf{DA} \right] \tilde{\mathbf{q}} \tag{17}$$

where the matrices $\mathbf{D}$ and $\mathbf{C}$ have dimensions $[M \times N]$, while $\mathbf{A}$ and $\mathbf{B}$ are $[N \times M]$, and their components are defined as

$$\begin{cases} A_{nr} = -\dfrac{1}{\pi b} \displaystyle\int_{-1}^{1} \dfrac{\cos n\theta(\xi)}{\sqrt{1-\xi^2}} \dfrac{\partial \psi_r(\xi)}{\partial \xi} \mathrm{d}\xi \\ B_{nr} = -\dfrac{1}{\pi b} \displaystyle\int_{-1}^{1} \dfrac{\cos n\theta(\xi)}{\sqrt{1-\xi^2}} \psi_r(\xi) \mathrm{d}\xi \\ C_{m0} = \displaystyle\int_{-1}^{1} \sqrt{1-\xi^2}\, \psi_m(\xi) \mathrm{d}\xi \\ C_{m1} = \displaystyle\int_{-1}^{1} \xi \sqrt{1-\xi^2}\, \psi_m(\xi) \mathrm{d}\xi \\ C_{mn} = \displaystyle\int_{-1}^{1} \left(\dfrac{\sin\left[(n+1)\theta(\xi)\right]}{(n+1)} - \dfrac{\sin\left[(n-1)\theta(\xi)\right]}{(n-1)} \right) \psi_m(\xi) \mathrm{d}\xi \quad \text{for } n > 1 \\ D_{m0} = 0 \\ D_{m1} = \displaystyle\int_{-1}^{1} (2\xi + 1) \dfrac{\sqrt{1-\xi}}{\sqrt{1+\xi}} \psi_m(\xi) \mathrm{d}\xi \\ D_{mn} = 2 \displaystyle\int_{-1}^{1} \sin n\theta(\xi)\, \psi_m(\xi) \mathrm{d}\xi \qquad \text{for } n > 1 \end{cases} \tag{18}$$

Finally, combining Eqs. (15) and (17) and performing the inverse Fourier transform we get the following definition in the time domain

$$\begin{cases} \mathbf{f}(\tau) = 2b\rho V^2 \left[\mathbf{CB}\ddot{\mathbf{q}} + (\mathbf{CA} + \mathbf{DB})\dot{\mathbf{q}} + \mathbf{DAq} \right. \\ \qquad \left. + \mathbf{g} \left(\ddot{r} - (z_1 + z_2)\dot{r} + z_1 z_2 r \right) \right] \\ \ddot{r} - (\sigma_1 + \sigma_2)\dot{r} + \sigma_1 \sigma_2 r = \mathbf{l}^T \dot{\mathbf{q}} + \mathbf{h}^T \mathbf{q} \end{cases} \tag{19}$$

where τ is the non-dimensional time variable, defined as $\tau = tV/b$. This expression of the aerodynamic loads is the key element of the proposed approach, which derives from the rational approximation of the lift deficiency function in Eq. (12) and represents a time-domain, state-space formulation applicable to free-wake, aeroelastic applications.
Note that, the velocity coefficients $\tilde{P}_n$ in Eq. (4) can be determined for arbitrary distributions of downwash, not necessarily produced by body motion. Thus, this formulation is well suited for the analysis of rotorcraft configurations where a fundamental contribution to downwash is typically given by the wake inflow.

Unsteady Kutta-Joukowski Theorem

The canonical formulation for lifting-line models exploits the widely-known Glauert formulation and Kutta-Joukowski theorem (Refs. 1, 21). Using this formulation in a time-stepping simulation tool including wake effects would result in a quasi-steady approach. In this case, to achieve the balance between circulatory lift and released vorticity, there is the need to iteratively modify the bound circulation, Γ, until appropriate matching is reached. To take into account the unsteady effects in this approach, the Kutta-Joukowski theorem extended to unsteady linear aerodynamics must be used (Ref. 14). Indeed, for each section of the wing, the following relation holds

$$\tilde{\Gamma} = \frac{1}{\rho V} H(k) \tilde{L}_c \tag{20}$$

where $H(k)$ represents the reciprocal of the Kutta-Joukowski frequency response function, which is given in terms of transcendental functions (namely Bessel functions) of the reduced frequency (Ref. 14), making it unsuitable for deriving state-space time-domain formulations. To achieve this objective, it is convenient to express it through an approximated rational form. Since $H(k) \to 0$ as $k \to \infty$, for the bound circulation frequency response function this expression can be used (considering $N_H > M_H$)

$$H(k) \cong H_0 \frac{\prod_{m=1}^{M_H}(ik - z_m)}{\prod_{n=1}^{N_H}(ik - p_n)} \tag{21}$$

where the constant H_0, the N_H poles p_n, and the M_H zeroes z_m are determined to obtain an adequate accuracy. Combining Eq. (21) with (20) and performing the inverse Fourier transform yields the following expression (Ref. 14)

$$\begin{cases} \Gamma(\tau) = \dfrac{1}{\rho V} \displaystyle\sum_{n=1}^{N_H} c_n r_n(\tau) \\ \dot{r}_n(\tau) = p_n r_n(\tau) + L_c(\tau) \qquad n = 1, \dots, N_H \end{cases} . \tag{22}$$

which provides, in nondimensional time τ, the bound circulation as a function of the circulatory lift time history (with the coefficients c_n obtained from the partial fraction decomposition). The added states r_n are introduced by the poles of the rational approximation. In the method developed for this study, $M_H = 3$ and $N_H = 4$ showed a satisfactory correlation with the exact solution through the entire range of application of the reduced frequency k. Note that the application of lower-order rational forms for the description of the function $H(k)$ would decrease the quality of the approximation, while not reducing significantly the computational cost of the proposed formulation. It is worth noting that a finite-state approximation of unsteady aerodynamic formulations can be found since the work of (Ref. 22). Thereafter, several approaches have been developed for the finite-state modeling of airfoil unsteady aerodynamics, many of which are outlined and compared in (Ref. 23). From that study can be gathered that the number of states introduced by this present finite-state approximation of the Kutta–Joukowski theorem is in line with the number of states typically introduced for lift response modeling.

Three-Dimensional Formulation

To include three-dimensional effects into the sectional solution via Küssner-Schwarz's model, it becomes necessary to take into account the effects of the velocity induced by the wake vorticity. Specifically, this contribution is included by numerically evaluating its chordwise distribution due to the trailing vortices (the effects from the shed vortices are already taken into account by the Küssner-Schwarz's theory). Dividing the wing into a prescribed number, N_B, of finite sections, discretizing the wake into N_W streamwise elements (eventually corresponding to the number of timesteps of the simulation), and evaluating the normal component of the induced velocity, v_i, at N_C collocation points along the chord of each section, it is possible to extend Eq. (1) as

$$v = V\frac{\partial w}{\partial x} + \dot{w} + v_i \tag{23}$$

thus extending correspondingly the definition of the coefficients P_n in Eq. (4), the pressure jump distribution, and the generalized aerodynamic loads. Overall, the contribution of the induced velocity modifies Eq. (19) as

$$\begin{cases} \mathbf{f}(\tau) = 2b\rho V^2 \left[\mathbf{CB}\ddot{\mathbf{q}} + (\mathbf{CA} + \mathbf{DB})\dot{\mathbf{q}} + \mathbf{DAq} + \mathbf{C}\dot{\mathbf{t}} + \mathbf{Dt} \right. \\ \qquad \left. + \, \mathbf{g}\left(\ddot{r} - (z_1 + z_2)\dot{r} + z_1 z_2 r\right)\right] \\ \ddot{r} - (\sigma_1 + \sigma_2)\dot{r} + \sigma_1\sigma_2 r = \mathbf{l}^T\dot{\mathbf{q}} + \mathbf{h}^T\mathbf{q} + \gamma \end{cases} \tag{24}$$

where $\mathbf{t}$ is a $N-$component vector and γ is a scalar whose expressions are given by

$$\begin{cases} t_n(y,t) & = -\dfrac{1}{\pi V}\displaystyle\int_{-1}^{1} \frac{\cos n\theta(\xi)}{\sqrt{1-\xi^2}}\, v_i\left(x(\xi), y, t\right) \mathrm{d}\xi \\ \gamma(y,t) & = -\dfrac{1}{\pi V}\displaystyle\int_{-1}^{1} \frac{\sqrt{1-\xi^2}}{1-\xi}\, v_i(x(\xi), y, t) \mathrm{d}\xi \\ & \qquad\qquad \text{for } n = 0, 1, \dots, N \end{cases} \tag{25}$$

The suitable integration of sectional loads given in Eq. (24) along the span gives the total (generalized) loads acting over the body (to be used, eventually, for aeroelastic analysis).

Time-stepping Formulation

In time-marching algorithms for unsteady aerodynamic simulations, each temporal increment necessitates iterative convergence prior to advancing the simulation time coordinate. Convergence is herein defined based on the sectional circulation: specifically, the iterative update process continues until the change in circulation, attributed to the lift contribution of newly shed wake elements during the iteration, is reduced below a predetermined tolerance.

At the onset of each time step, sectional aerodynamic forces are computed employing the Küssner-Schwarz's model. These forces incorporate contributions from freestream, kinematic, and induced velocities. Initially, the induced velocity field is reconstructed exclusively from wake elements released during previous time steps. The computations are performed independently for each airfoil section.
Subsequently, the updated sectional circulatory lift is input into an unsteady Kutta–Joukowsky augmented-state model, which produces an updated distribution of bound circulation along the wing span. Once the bound circulation is determined across all sections, a new wake line is released. Since the introduction of this new wake elements modifies the flow field responsible for its generation, the induced velocity field must be corrected accordingly.
This correction of induced velocities initiates a renewed evaluation of sectional aerodynamic forces, bound circulation, and wake shedding (as shown in 1). The iterative

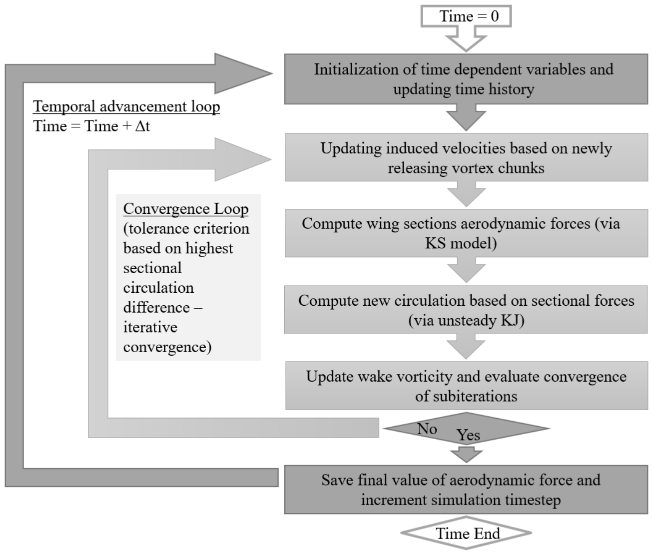

Figure 1. Temporal Advancement Scheme

cycle, comprising the recomputation of aerodynamic forces, the update of the bound circulation, the release of the wake and the induced velocity correction, is repeated until the normalized variation in the sectional circulation between successive iterations falls below the convergence criterion. Upon achieving convergence, the simulation time is incremented, the wake is convected downstream, and the procedure is reiterated for the subsequent time step.

Extension to Rotary Wing Aerodynamics

The formulation described above can be directly applied for the simulation of unsteady aerodynamics of translating wings. Note that, in the case of a non-rectangular planform, attention must be paid to the spanwise variation of reduced frequency. Indeed, in that case, once defined a global reduced frequency through which the wing dynamic is described, different local sectional reduced frequency require an appropriate re-scaling of the sectional aerodynamic formulations, including re-scaling of zeroes and poles of the rational approximations of lift deficiency function and Kutta-Joukowski transfer function (Ref. 24).

However, the application of the presented unsteady aerodynamic formulation can be also extended to rotors in hovering or axial flight. In this case, the spanwise variation of the sectional reduced frequency occurs regardless of the blade planform, and is due to the radial variation of the undisturbed flow velocity (for instance, $V = \Omega r$ in hovering flight, with Ω and r denoting, respectively, rotor angular speed and radial position of the section). Therefore, a global reduced frequency is introduced and local re-scaling of the reduced frequency is applied as already mentioned for the fixed wing case. In addition, for rotor configurations, the shape of the wake is assigned a priori (for instance, as a simple helical surface, or through the application of a semi-empirical model) with the pitch defined in terms of the thrust coefficient, or evaluated as a result of the self-induced velocity in a free-wake solution mode (Ref. 24).

NUMERICAL RESULTS

This section begins by evaluating the accuracy of the proposed ULLT formulation for estimating integral unsteady rotor loads produced by blade motion. The assessment is made through a comparison with predictions from a BEM computational tool, which models three-dimensional lifting bodies in arbitrary motion. It is important to note that this tool has been thoroughly validated against both experimental and numerical data from literature, covering fixed and rotary wing configurations (Refs. 5–12).

The numerical results presented consider the thrust time history induced by both blade pitch and flap deflections, derived through time-marching simulations. The impact of wake modeling on load predictions is examined.

In the main results presented hereafter, the performances of three aerodynamic simulation codes will be compared: the proposed ULLT formulation (USLL), the aforementioned BEM, and a standard lifting line formulation (LL), based on Prandtl-Glauert model, with a full panel wake. It is important also to point out the latter does feature the inclusion of added mass terms for noncirculatory lift, and it is introduced to show the increase in accuracy given by the enhancements developed in the proposed ULLT.

Each code can model the rotor's wake as a fixed helical surface, with the spiral length explicitly determined by the inflow parameters. This ensures that the wake, which strongly affects rotor aerodynamics, maintains the same influence across all simulations. Indeed, by employing an identical fixed wake configuration, any observed differences in the simulation outcomes can be attributed solely to the intrinsic aerodynamic formulation of the respective codes, thereby enabling a fair and rigorous comparative analysis.

Before data acquisition, the different solvers were brought to convergence to obtain the best possible results with reference to the data available for the rotor studied (Ref. 25). In particular, the rotor considered is a 40% scaled version of the *BO105* main rotor. It is a four-bladed rotor with a radius of $R = 2.0$ m and rectangular blades. Such blades are built using a *NACA23012* airfoil and a linear twist of $\theta = -4.0$ deg/m. This preliminary test helped assess the basic functionality of the codes in steady conditions, set the proper number of wake spirals to achieve convergence and establish the spanwise and chordwise discretization required.

The reference thrust and torque value from the experimental reference are 3254 N and 457 Nm, respectively; the BEM results achieves 3280 N of thrust and 451 Nm of torque, while the ULLT method achieves 3246 N of thrust and 456 Nm of torque - same values achieved with the LL model (which is to be expected in steady conditions). All codes have the additional contribution of the parasite drag mediated by the estimation of the rotor airfoil via *XFOIL* simulations in viscous mode at dedicated Mach numbers.

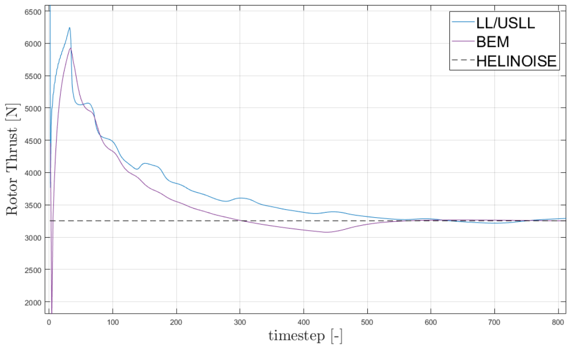

Figure 2. Time History Steady Hovering Simulation

Table 1. Reference Rotor Characteristics

Radius	2.0 m
Chord	0.121 m
Twist Ratio	4.0 deg/m
Null Twist	@0.75R
Cutout	0.25R
Airfoil	NACA0012
Rotational Speed	1041 RPM
Reference Collective Pitch	5.0 deg

The rotor used for the harmonic hover tests listed afterwards is described in 1.

The blade discretization plays a fundamental role in the aerodynamic loads prediction. The spanwise discretization, namely the number of aerodynamic sections considered, achieved convergence at $\sim$ 30 sections for all three solvers. On the other hand, the chordwise discretization is naturally different for all solvers; the BEM solver achieved convergence at $\sim$ 60 panels along the airfoil line, while the USLL required $\sim$ 80 nodes to converge on the unsteady loads (in steady cases, ideally one point is sufficient and the solution reduces to a Theodorsen-like formulation). The LL solver naturally does not feature this possibility. It is worth reminding that the USLL chordwise discretization is simply a series of spatial probes for induced velocity, spaced across the airfoil mean line, and do not play a role in the potential solution as they would, for instance, in a lifting surface model.

The temporal convergence achieved optimal results for a timestep equal to 2.5° of azimuthal step. The most critical situation for the simulations was the passage of the following blade over the wake released by the preceding one: a reduced length of the vortex chunks with respect to the mean blade chord helps stabilize the induced velocity contribution and achieving solution stability.

Analysis of Blade Harmonic Pitching in Hovering

The rotor setup is now investigated under unsteady conditions to evaluate the accuracy of the newly developed solver in comparison with the benchmark BEM solver and the reference LL implementation. From an average collective pitch value of 5°, the blades are then subjected to a collective pitch sinusoidal variation of 1° of amplitude.

For the blade pitching frequency $\omega_p = 2$/rev and rotor in hovering condition, Fig. 3 shows the temporal histories of rotor thrust predicted by the proposed USLL, the BEM solver and the standard LL model.

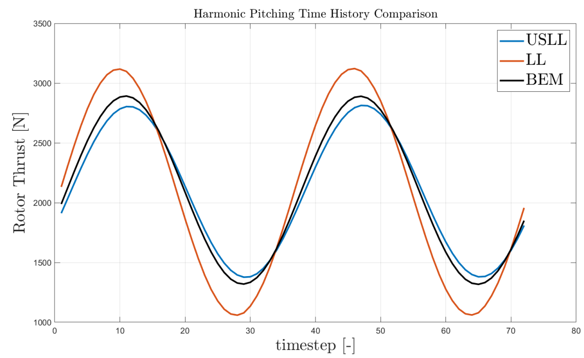

Figure 3. Thrust due to 2/rev harmonic pitching. Hovering flight.

It is immediate to notice the staggering enhancements of the USLL solution with respect to the canonical lifting line. The average thrust magnitude is better captured, but most importantly the phase of the load peaks are better resembling the ones in the BEM solution. This results is especially meaningful keeping in mind that lifting line solvers are mainly developed for multiphysics simulations, where the frequency response becomes fundamental to evaluate the aeroelastic stability of the system.

Next, Figs. 4 and 5 illustrate the comparisons among thrust predictions given by USLL, BEM and LL solvers, respectively for $\omega_p = 1$/rev and $\omega_p = 4$/rev. These demonstrate that the newly developed model maintains its performance superiority over the standard LL formulation even for lower and higher pitching frequencies.

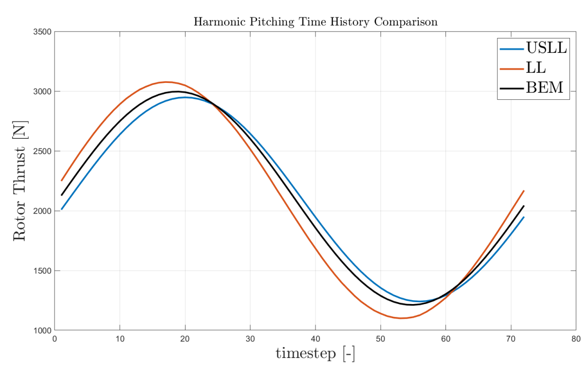

Figure 4. Thrust due to 1/rev harmonic pitching. Hovering flight.

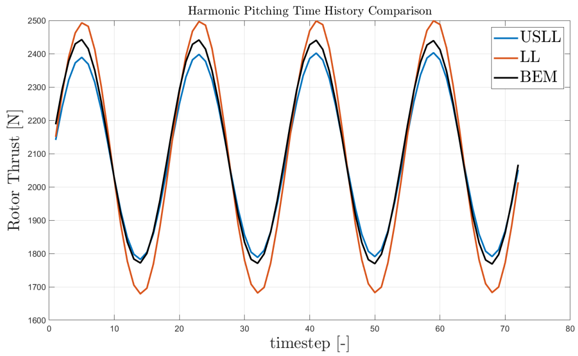

Figure 5. Thrust due to 4/rev harmonic pitching. Hovering flight.

This consistent behavior indicates that the innovations of the USLL model make it able to capture accurately a wide unsteady aerodynamics frequency range.

Analysis of Blade Harmonic Flapping in Hovering

The investigation on the rotor under unsteady conditions proceeds also for flapping motion. Still considering an average collective pitch value of 5°, the blades are then subjected to a sinusoidal collective rigid flapping motion with tip displacement amplitude equal to 0.01 m, and frequency equal $\omega_f = 2$/rev.
Temporal histories of rotor thrust for a whole revolution given by USLL, BEM and LL solvers are depicted in Fig. 6. Also in this case the USLL solution is in good agreement with BEM ones, significantly improving the predictions provided by the standard LL model.

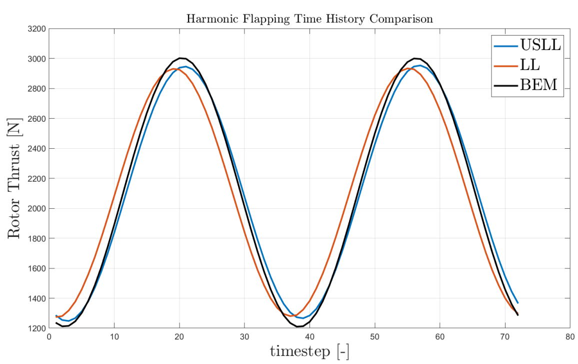

Figure 6. Thrust due to 2/rev harmonic flapping. Hovering flight.

Free Wake Analysis

Free wake simulation offers significant advantages over fixed wake approaches by dynamically capturing the evolution of the rotor wake's vortex structures. Unlike fixed wake models, which assume a stationary wake configuration, free wake formulations account for the convective and deformable nature of the vortical flow, revealing intricate wake topologies, inherent asymmetries, and evolving patterns that a static model would overlook (see Fig. 7). While the predictions of overall loads integrals, such as thrust and moment, is marginally affected by the adoption of free-wake solution, the detailed wake characterization provided by the free wake model is critical. It qualitatively demonstrates that a body interacting with the wake could experience highly non-uniform and localized load distributions. Such insights are essential for understanding complex rotor–body interactions, enabling more accurate assessments of aerodynamic performance and structural responses in realistic operating conditions (like those with BVI occurrence).

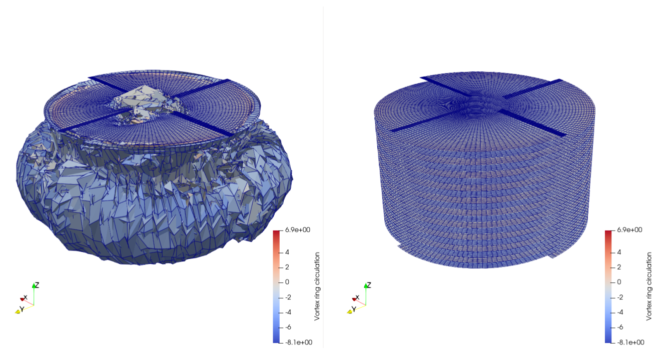

Figure 7. Wake topologies for blade harmonic pitching in hovering flight (colored with circulation).

Figure 7 represents the wake structures after 5 revolutions, where it is possible to observe the secondary flow patterns, such as the fountain effect at the rotor center.

Axial Flight

The proprotor operating in a predominantly axial-flow regime — typical of high advance ratio forward flight — provides an ideal validation case for tilt-rotor aerodynamic solvers by introducing the key physical phenomena that complicate tilt-rotor aerodynamics. In this regime, wake behavior is characterized by significant skewing and contraction, necessitating accurate prediction of wake tip vortices. Unlike hover conditions where freestream velocity is negligible, axial-flow forward flight challenges solvers to correctly superimpose freestream and induced flows, providing a transitional benchmark between hover and airplane-mode simulations.

The proprotor described in 2 is the subject of this last set of results, where the application test case changes from hover conditions to forward axial flight condition, when most of the inflow velocity is provided by the advancing motion of the aircraft.
Just like the rotor case, the propeller geometry was at first evaluated in steady conditions to assess the numerical convergence of space and time discretization, and then verified in

Table 2. Reference Proprotor Characteristics

Radius	3.6 m
Chord	0.250 m
Twist Ratio	7.64 deg/m
Null Twist	@0.75R
Cutout	0.25R
Airfoil	NACA0012
Rotational Speed	300 RPM
Reference Cruise Speed	200 keas
Reference Collective Pitch	55.0 deg

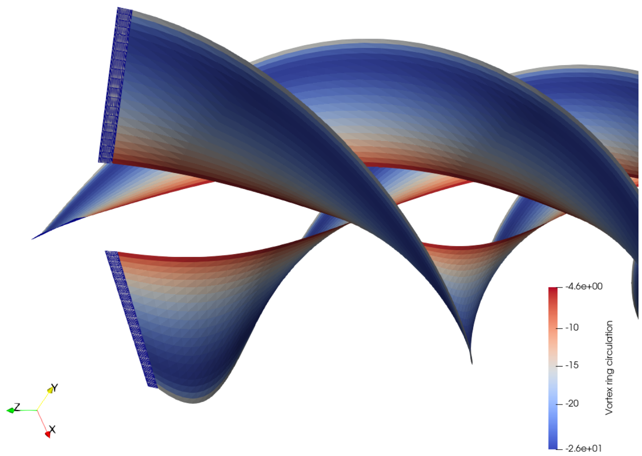

Figure 8. Proprotor reference wake topology (colored with circulation).

unsteady applications. The latter consists of blade harmonic pitching around a reference collective pitch value of 55°, with amplitude equal to 1° and frequency equal to $\omega_p = 2$/rev.

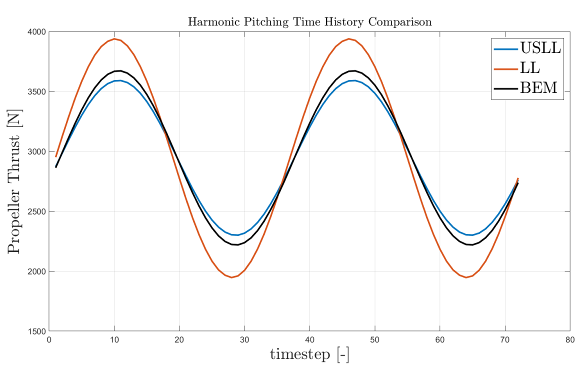

Figure 9. Proprotor thrust due to 2/rev harmonic pitching.

In Fig. 9 the harmonic thrust curves clearly demonstrate the unsteady nature of the propeller loading, as all three models oscillate in time. However, the newly developed USLL model tracks the BEM benchmark almost exactly — in both amplitude and phase — whereas the standard LL solution significantly underestimates the peak-to-peak thrust and exhibits a pronounced phase lag. This close alignment of USLL with the BEM reference underscores its superior capability to capture the true unsteady thrust dynamics.

It is worth reminding that one of the principal distinctions between an axial-flight propeller and a hovering rotor emerges when their dynamics are formulated in terms of generalized Lagrangian coordinates. In the hovering case, the undisturbed flow velocity is effectively zero, which simplifies the mapping between the blade-fixed reference frame and the inertial frame. By contrast, an axial-flight propeller operates in a nonzero freestream, so its generalized coordinates must be defined with respect to the undisturbed inflow velocity. Hence, explicitly accounting for the axial flight speed within the coordinate definition is essential for accurately capturing the coupling between blade motion and incoming flow in forward flight.

CONCLUSIONS

The newly developed unsteady lifting line method presented here is capable of providing reliable results for unsteady rotor flight conditions, enhancing the capabilities of standard lifting-line formulations. Exploiting a frequency-domain sectional analytical solution suitable for arbitrary airfoil motion, and reformulating it in time domain by proper scaling of reduced frequency, it is possible to simulate rotary wings with an unprecedented accuracy for this kind of modeling, making it suitable for multiphysics applications. For proprotors applications, the proposed USLL accurately captures transient aerodynamic loads encountered during mode transitions. This fidelity is critical for potential realistic drivetrain torque estimation, gearbox fatigue analysis, and control system tuning. Furthermore, USLL's ability to resolve unsteady thrust spikes improves predictions of blade vibration and acoustic emissions. In aero-servo-elastic simulations, USLL's accurate phase and amplitude alignment ensures more reliable flutter assessments and informed control-law development. Additionally, its computational efficiency makes it well-suited for real-time simulation environments and hardware-in-the-loop testing, positioning it as a robust tool for future digital twin and advanced flight control architectures. In terms of computational performance, in fact, the USLL model is also in this case ∼10 times faster to perform this kind of analysis on the same hardware architecture used for a BEM simulation, with a risible increment with respect to the standard LL simulation.

Author contact: Gregorio Frassoldati
gregorio.frassoldati@uniroma3.com
gregorio.frassoldati@leonardo.com

REFERENCES

1. H. Glauert. *The Elements of Aerofoil and Airscrew Theory*. Cambridge Science Classics. Cambridge University Press, 1948.

2. L. Prandtl. Applications of modern hydrodynamics to aeronautics. NACA TR-116, 1923.

3. T. Theodorsen. General theory of aerodynamic instability and the mechanism of flutter. NACA TR-496, 1935.

4. Herbert Wagner. Über die entstehung des dynamischen auftriebes von tragflügeln. *ZAMM - Journal of Applied Mathematics and Mechanics / Zeitschrift für Angewandte Mathematik und Mechanik*, 5(1):17–35, 1925.

5. L Morino and M Gennaretti. Boundary integral equation methods for aerodynamics. In S N. Atluri, editor, in *Computational Nonlinear Mechanics in Aerospace Engineering*, Progress in Astronautics and Aeronautics Series, Vol. 146, pages 279–320. AIAA, Washington, DC, 1992.

6. M. Gennaretti, F. Salvatore, and L. Morino. Forces and moments in incompressible quasi-potential flows. *Journal of Fluids and Structures*, 10(3):281–303, 1996.

7. G. Bernardini, F. Salvatore, M. Gennaretti, and L. Morino. Viscous/potential interaction for the evaluation of airloads of complex wing systems. In *XIV AIDAA Congress, Naples, Italy*, pages 53–62, 1997.

8. M Gennaretti, L. Luceri, and L Morino. A unified boundary integral methodology for aerodynamics and aeroacoustics of rotors. *Journal of Sound and Vibration*, 200(4):467–489, 1997.

9. M. Gennaretti, G. Calcagno, A. Zamboni, and L. Morino. A high order boundary element formulation for potential incompressible aerodynamics. *The Aeronautical Journal (1968)*, 102(1014):211–219, 1998.

10. Luigi Morino and Giovanni Bernardini. Singularities in bies for the laplace equation; joukowski trailing-edge conjecture revisited. *Engineering Analysis with Boundary Elements*, 25(9):805–818, 2001.

11. L. Morino and G. Bernardini. Recent developments on a boundary element method in aerodynamics. In Tadeusz Burczynski, editor, *IUTAM/IACM/IABEM Symposium on Advanced Mathematical and Computational Mechanics Aspects of the Boundary Element Method*, pages 237–247, Dordrecht, 2001. Springer Netherlands.

12. M Gennaretti, G Bernardini, J Serafini, and G Romani. Rotorcraft comprehensive code assessment for blade-vortex interaction conditions. *Aerospace Science and Technology*, 80:232–246, 2018.

13. M. Gennaretti and G. Bernardini. Novel boundary integral formulation for blade-vortex interaction aerodynamics of helicopter rotors. *AIAA Journal*, 45(6):1169–1176, 2007.

14. Massimo Gennaretti and Riccardo Giansante. Kutta–joukowski theorem for unsteady linear aerodynamics. *AIAA Journal*, 60(10):5779–5790, 2022.

15. H.G. Küssner and I. Schwarz. The oscillating wing with aerodynamically balanced elevator. Technical Report No.991, NACA, 1941.

16. Y.C. Fung. *An Introduction to the Theory of Aeroelasticity*. Dover Publications, Inc., New York, 1993.

17. W. R. Sears. Some aspects of non-stationary airfoil theory and its practical application. *Journal of Aeronautical Sciences*, 8(3):104–108, 1941.

18. J.P. Giesing, W.P. Rodden, and B. Stahl. Sears function and lifting surface theory for harmonic gust fields. *Journal of Aircraft*, 7(3):252–255, 1970.

19. H. G. Küssner. Summary report on the nonstationary lift of wings. volume 13, pages 410–424. 1936.

20. C Venkatesan and Peretz P Friedmann. New approach to finite-state modeling of unsteady aerodynamics. *AIAA Journal*, 24(12):1889–1897, 1986.

21. Joseph Katz and Allen Plotkin. *Low-Speed Aerodynamics*. Cambridge Aerospace Series. Cambridge University Press, 2 edition, 2001.

22. R. Jones. “operational treatment of the nonuniform lift theory to airplane dynamics. NACA TN-667, 1938.

23. D. A. Peters. Two-dimensional incompressible unsteady airfoil theory — an overview. *Journal of Fluids and Structures*, 24(3):295–312, 2008.

24. M Gennaretti. *Fundamentals of Aeroelasticity*. Springer Nature, Switzerland AG, 2024.

25. H. Heller, W. Splettstoesser, V. Kloeppel, and F. Cenedese. Helinoise - the european community rotor acoustics research program. *AIAA Journal*, 1993.